High-Pressure Pulsing of Ammonia Results in Carbamate as Strongly Inhibiting Adsorbate of Methanol Synthesis over $Cu/ZnO/Al_2O_3$

Benjamin Mockenhaupt, Philipp Schwiderowski, Jelena Jelic, Felix Studt, Martin Muhler, and Malte Behrens*

ABSTRACT: The active site of the industrially used Cu/ZnO catalyst for the formation of methanol is controversially debated to date. Ammonia has been used as a probe molecule as it was found to inhibit methanol synthesis in CO_2-containing synthesis gas. Herein, we investigate the poisoning effect using an industrial-type $Cu/ZnO/Al_2O_3$ catalyst synthesized by co-precipitation. During steady-state methanol synthesis in a $CO_2/CO/H_2$ synthesis gas, isobaric trimethylamine (TMA) and ammonia injections poisoned methanol formation reversibly, with the poisoning of ammonia being significantly stronger than that of TMA. Based on DFT calculations, a mechanism of ammonia poisoning was derived: ammonia activation takes place on adsorbed oxygen or hydroxyl groups, followed by the reaction with CO_2 forming a stable carbamate on the active site. Further hydrogenation of the carbamate to methylamine was calculated to exhibit high barriers, thus being rather slow, explaining why ammonia poisoning has a long-term effect, as TMA cannot form a strongly bound carbamate species exclusively acting as weakly bound site-blocking species.

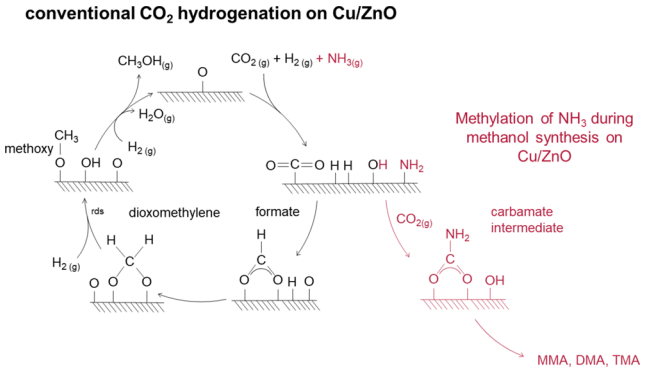

INTRODUCTION

The industrial methanol synthesis process currently received great attention again because of the promising potential in the power-to-liquid concepts for the mitigation of greenhouse gas emissions and as an alternative to fossil energy carriers. Methanol is in particular interesting because it can be used both in the fuel and the chemistry sectors.[1−5]

Industrially, methanol is synthesized from syngas mixture containing CO, CO_2, and H_2 at pressures of 50−100 bar and temperatures of 200−300 °C over Cu-/ZnO-based catalysts.[6] As in many industrial catalytic processes, the technological application of methanol synthesis has preceded the full understanding of the underlying chemistry, which has led to a vast amount of empirical knowledge that has been complemented by the growing fundamental and mechanistic insights in the last decades.[5,7] However, the exact detailed reaction mechanism, the nature of the active sites of high-performance catalysts, and the interplay of the catalyst's surface with the feed gas components are debated to this day.[8−10] Among the most important open question is the dynamic effect of the so-called "Cu−Zn synergy" on the nature of the active site responsible for methanol formation.[11] New experiments and calculations allow a more detailed understanding, which could be key to a knowledge-based adaptation of the current industrial process for future power-to-methanol applications.

For example, the zinc coverage on the copper nanoparticle was interpreted as a surface alloy, which strongly affects the methanol synthesis activity of the catalyst and can be determined by chemisorption methods.[12,13] This behavior may be due to an enhanced methanol formation route via zinc formate determined by spectroscopy with isotopic labeled carbon dioxide sources.[14] Nevertheless, the change of the catalyst surface, and in particular the oxidation state of Zn, depends strongly on the redox potential of the gas phase. At rather oxidizing conditions (CO_2-rich), oxidized Zn^{2+} in Cu/ZnO can be assumed, which changes at reducing conditions (CO-rich) via $Cu−Zn^{\delta+}$ to a Cu−Zn surface alloy, for which ZnO acts as a Zn reservoir.[14,15] Hence, the catalyst is typically activated under strongly reducing conditions (H_2 in inert gas and 250 °C), and the Cu−Zn surface alloy and the activated $Cu−Zn^{\delta+}$ interface site are likely candidates for the active site in methanol formation from carbon dioxide.[15] This surface alloy is found to coexist with ZnO_x islands, and thus with the $Cu−Zn^{\delta+}$ interface sites, after the catalyst activation at

temperatures in the range of 200−340 °C. At temperatures above 340 °C, a bulk brass alloy is formed by the continuous consumption of the zinc oxide species, which are in close contact with the copper particles.[16]

Recently, a new experimental approach for the surface characterization of the working $Cu/ZnO/Al_2O_3$ catalysts has been presented. Laudenschleger et al.[17] introduced high-pressure pulses of ammonia (NH_3) as a new tool to probe the active site of an industrial $Cu/ZnO/Al_2O_3$ catalyst during methanol synthesis. This method complements the traditional ex situ chemisorption methods based on N_2O decomposition and hydrogen temperature-programmed desorption (H_2-TPD). These have already shown that depending on the catalyst composition and the used feed gas, a linear relationship between the copper surface area and the activity in methanol synthesis is observed. The contribution of partially reduced zinc oxide to the N_2O decomposition capacity, however, increases the complexity to accurately characterize the catalyst surface,[13,18,19] as the amount of reduced zinc oxide will depend on the pretreatment conditions[13,16] at low temperature and might not represent the working state of the catalyst.[20]

Contrary to these chemisorption methods, the new *operando* ammonia pulse experiments are conducted on the working catalyst, and the first results confirmed the important role of $Cu-Zn^{\delta+}$ interface sites.[17] The upstream isobaric injection of ammonia leads to a sudden temporary poisoning of methanol formation. The linear increase of poisoning strength as a function of CO_2 content in the synthesis gas and the absence of poisoning of the parallel ethylene hydrogenation probe reaction as well as that of pure CO hydrogenation, both of which are considered to take place on the unpromoted Cu^0 sites, make this method sensitive to the $Zn^{\delta+}$-promoted CO_2 conversion sites on the Cu/ZnO catalyst.[17]

Ammonia introduced as pulses was observed to be converted to trimethylamine (TMA). Here, we report experiments using a well-characterized highly active $Cu/ZnO/Al_2O_3$ methanol synthesis catalyst of academic origin. This is a reproduction of a benchmark catalyst whose synthesis history and structural properties are fully disclosed and thus allow for the establishment of structure−activity correlations. Furthermore, we combine the experimental data with density functional theory (DFT) to identify the reaction mechanism of TMA formation, especially to uncover its active site, which leads to poisoning of methanol formation, thus being identical to the active site for CO_2 hydrogenation to methanol.

METHODS

Catalyst Synthesis and Characterization. The investigated catalyst is an alumina-promoted copper/zinc oxide catalyst that was self-prepared from a co-precipitated precursor using a preparation recipe that was inspired by the established industrial synthesis. It is composed of precursor co-precipitation, aging in the mother liquor, recovery, calcination in air, and finally reduction in a diluted hydrogen stream directly prior to the catalytic experiments. Its synthesis was a reproduction of the catalyst described earlier as Cu/ZnO:Al, which itself has been the subject of several studies or has been used as a benchmark catalyst for activity comparisons, and is here abbreviated CZA. In more details, the precursor of the investigated catalyst was synthesized via co-precipitation according to Schumann et al.[21] The precipitation was carried out in an automated stirred tank reactor (OptiMax, Mettler Toledo) from 1 M metal salt nitrate solution at a temperature of 65 °C. During the precipitation with 1.6 M sodium carbonate solution and using a dosing rate of 2.5 g min^{-1}, the pH was held constant at 6.5. Afterward, the co-precipitate was aged in its mother liquid without further pH control. After the typical pH drop[21] had been observed, aging was continued for 1 h. In a following procedure, the precursor was washed with deionized water 15 times to remove the sodium and nitrate ions, followed by drying the precipitate in a heating chamber at 80 °C overnight. The recovered powder was grinded and afterward calcined at 350 °C for 3 h using a heating ramp of 2 °C min^{-1} in a muffle furnace with static air. The calcination temperature deviates from the procedure described by Schumann et al.,[21] and their catalyst is denoted FHI-Std., for which 330 °C has been used. The increase of the calcination temperature by 20 °C was necessary for a more complete decomposition of the hydroxycarbonate precursor but may come at the cost of a slightly lower specific surface area due to stronger sintering (Table 1).

Table 1. Characterization of the Self-Prepared CZA (Cu/ZnO:Al) Catalyst in Comparison to the Published Commercial CZA and FHI-Std. Benchmark Catalyst[a]

catalyst property	CZA (Cu/ZnO:Al) of this study	commercial CZA reported by Laudenschleger et al.[17]	FHI-Std. reported by Schumann et al.[21]
$A_{BET}/m^2\ g^{-1}$	93	NA	118
$A_{Cu}/m^2\ g^{-1}$[b]	27	28	38
$D_{Cu}/\%$[b]	18	NA	8
d_{Cu}/nm[c]	7	NA	4.47
$T_{max,reduction}/°C$	170	170	211

[a]The BET surface area (A_{BET}) was measured by N_2 physisorption. [b]The Cu surface area (A_{Cu}) and the -dispersion (D_{Cu}) are calculated from the N_2O-RFC method. [c]The Cu crystallite size (d_{Cu}) was determined by applying the Scherrer equation to the 111 reflection and by Rietveld refinement for the FHI-Std. catalyst.[21] The temperature with the maximum hydrogen consumption rate ($T_{max,reduction}$) was determined from the TPR profile with a heating rate of 1 °C min^{-1} (CZA) and 6 °C min^{-1} (FHI-Std.[21]).

The metal composition was chosen as 68:29:3 in CZA. The co-precipitated precursor, the corresponding oxide, and the reduced catalyst were characterized by the following methods.

Atomic absorption spectroscopy (AAS) was performed on a Thermo Fisher iCE-3500 AAS instrument after dissolving the sample in nitric acid overnight. The nominal metal ratio was 68:29:3, and this is close to the experimentally found values of 69(+/−1.5):29(+/−1.4):2(+/−0.003).

Powder X-ray diffraction (XRD) patterns of the co-precipitated precursor and the calcined precatalyst were recorded on a Bruker D8 ADVANCE system in Bragg−Brentano geometry with a LYNXEYE XE-T detector using Cu K-alpha radiation. Phase analysis was performed using structural data from ICSD and COD databases.

Surface area analysis by the nitrogen physisorption of precursors and calcined samples was determined by applying the Brunauer−Emmett−Teller (BET) equation to the N_2 adsorption data in the range of 0.07−0.3 of the pressure ratio measured at −196 °C. The sample was first degassed under vacuum at 80 °C for 2 h to remove any adsorbates. The determination of the pore sizes was done by applying the Barrett−Joyner−Halenda (BJH) method to the desorption

isotherm. The measurement was carried out in a BET analysis setup with a NOVA 3200e of Quantachrome analyzer and analyzed with the NovaWin software.

Temperature-programmed reduction (TPR) of 100 mg of 250−355 μm sieve fraction was performed in a quartz glass U-shaped tube reactor with an inner diameter of about 4 mm. As a reducing atmosphere, 4.6% H_2 in Ar with a volume flow of 84.1 mL min^{-1} at ambient pressure was used. Starting from room temperature, the sample was heated up to 240 °C with a heating ramp of 1 °C min^{-1}. After reaching the target temperature, it was held for 30 min to ensure recording the complete reduction profile. The formed water during reduction was separated by a cooling trap to enable the analysis of the consumed H_2 via a thermal conductivity detector (Hydros 100).

N_2O reactive frontal chromatography (N_2O-RFC) was analyzed in a similar reactor with the same mass loading and sieve fraction as that used for TPR. Before recording the N_2O consumption, the sample was reduced in a gas containing 2.1% H_2 in He. To ensure a completely adsorbate-free surface, the reduced sample was treated for 1 h at 220 °C in a He stream, followed by cooling to room temperature. The N_2O decomposition experiment was performed with 1% N_2O in He at room temperature and atmospheric pressure. The consumption of N_2O was determined by a calibrated quadrupole mass spectrometer (Balzer GAM 400). Calculating the metal surface areas and other quantities related to N_2O-RFC was performed according to DIN 66136-1.[22]

Catalytic Testing and Ammonia Pulse Chemisorption. *Activation.* For activation, 200 mg of the catalyst in the sieve fraction of 255−350 μm was heated to 175 °C at a heating rate of 1 °C min^{-1} using a gas flow rate of 500 mL_N min^{-1} g_{cat}^{-1} of 2 vol % H_2 in N_2 for 15 h. Then, the temperature was increased to 240 °C with 1 °C min^{-1} and held for 30 min.

Aging of the Catalyst. To reach steady-state conditions in a relatively short period of time, the corresponding catalyst sample was aged before performing the kinetic experiments. For the investigation of the initial activity, the catalyst was run under kinetically controlled conditions in 13.5 vol % CO, 3.5 vol % CO_2, 73.5 vol % H_2, and 9.5 vol % N_2 syngas with a volume flow of 666 mL_N min^{-1} g_{cat}^{-1} at 210 °C and 60 bar for 1 week.

For the further aging process, the reaction temperature was set at 250 °C and the volume flow to the minimal possible value to reach equilibrium-controlled conditions to ensure a reproducible deactivation. By exposing the whole catalyst bed to high conversion conditions, according to the study of Fichtl et al.,[23] steady state was reached after another week.

High-Pressure Pulse Experiments with NH_3 and TMA. Similar to the aging process as for the standard syngas mixture, the following composition was used: 13.5 vol % CO, 3.5 vol % CO_2, 73.5 vol % H_2, and 9.5 vol % N_2. The kinetically controlled measurements were performed in the differential region at 210 °C and 60 bar with a syngas flow of 666 mL_N min^{-1} $g_{Catalyst}^{-1}$. A constant volume of 1 mL N_2 containing various mole fractions from 0 to 2000 ppm of NH_3 and TMA was injected into the upstream synthesis gas as isobaric pulses.

Density Functional Theory Calculations. DFT calculations were performed using the Vienna Ab Initio Simulation Package (VASP)[24−27] in connection with the atomic simulation environment (ASE).[28,29] The Bayesian error estimation functional with van der Waals correlations (BEEF−vdW)[30] with the projector augmented-wave method (PAW)[31,32] and a plane-wave basis set with a cutoff energy of 450 eV was used. The choice of the BEEF−vdW functional is motivated by its performance with respect to adsorption energies[33,34] and transition states[35] on transition metal surfaces and in particular by its successful description of surface processes related to CO_2 hydrogenation to methanol.[11,36]

Infinite slab models for Cu(211) termination consist of four-layer thick 3 × 3 supercells, separated by more than 16 Å in the z direction. Zinc-containing alloys were constructed by the substitution of Cu with Zn atoms along the Cu(211) edge (denoted ZnCu(211)). The bottom two layers were kept fixed, and the upper two layers were allowed to relax during geometry optimizations. The Brillouin zone was sampled using a 5 × 4 × 1 Monkhorst−Pack k-point grid[37] for both Cu(211) and ZnCu(211). The convergence criterion for the geometry optimizations was a maximum force of 0.01 eV/Å. Transition states were obtained using constrained optimizations. All transition states were verified to contain a single imaginary harmonic frequency corresponding to the transition vector of the reaction. All adsorption energies were corrected by zero-point energy (ZPE) contributions. Entropic contributions to the free energy were calculated within the harmonic approximation for adsorbates, and entropic contributions for gas-phase species were obtained from the tabulated values (see Supporting Information for all data). All optimized structures of adsorbates and transition states are given in the Supporting Information.

RESULTS AND DISCUSSION

Catalyst Characterization. The composition (Figure S1 and Table S1), the XRD patterns of the precursor (Figure S2) and that of the calcined form (Figure S3), the N_2 adsorption isotherms (Figure S4 and Table S2), the TPR curve (Figure S5a), and the N_2O-RFC profile (Figure S5b) of the CZA catalyst are presented in the Supporting Information. In agreement with previous results, XRD confirmed that the precursor of the catalyst mainly crystallized in a malachite structure (Figure S2) and that the typical by-phase[38] of Al-rich hydrotalcite is hardly observed but cannot be completely ruled out based on the powder patterns. The shift of the $20\bar{1}$ peak corresponds to a d-spacing of 2.754 Å and is in line with the results obtained by Schumann et al.[21] This value indicates a proper substitution of Cu^{2+} by Zn^{2+} and Al^{3+} cations. The calcination at 350 °C for 3 h resulted in the transformation to a poorly crystalline metal oxide mixture, and only a small crystalline residue of the malachite precursor phase was still present (Figure S3). The broad peak at $2\theta \approx 35°$ indicates a nanostructured CuO−ZnO composite, as expected for industrial-type catalyst synthesis.[21] The TPR experiment in 5% H_2 showed that the reduction of CuO to Cu^0 reached the maximum rate at 170 °C and was complete at 200 °C (Figure S5a). Relating the amount of Cu determined by AAS with the amount of consumed H_2, the degree of reduction was determined to be 100% after the TPR experiment.

After reduction, metallic Cu^0 and nanostructured ZnO were identified by XRD analysis (Figure S5c). According to a simple Scherrer analysis of the 111 reflection, the crystallite size of metallic copper was determined to amount to 7 nm, which is around 3 nm larger compared with that of Schumann et al.,[21] which may be due to the slightly harsher calcination conditions resulting in larger CuO crystallites. The reduced catalyst was also characterized by N_2O-RFC (Figure S5b), resulting in a

specific Cu metal surface area of 27 m^2 g^{-1} (Table 1). In relation to the BET surface of the oxide (93 m^2 g^{-1}), this value is almost one-third of the previous oxide surface area. The N_2O-RFC results of Cu/ZnO catalysts, however, must be interpreted carefully. Fichtl et al.[19] demonstrated that partially reduced ZnO_{1-x} (e.g., oxygen vacancies) in a Zn-containing catalyst does react with N_2O.[19] Partial reduction of ZnO that contributes to the N_2O chemisorption capacity was also reported by Kuld et al.[13] Therefore, Cu surface area and Cu dispersion may be overestimated and the crystallite size underestimated by N_2O data. This discussion is of high relevance when comparing different catalysts, but in this study on a single catalyst material, we refrain from a further interpretation of the N_2O-RFC data showing values that are in the range previously reported for industrial catalysts.[18,19]

Table 1 summarizes the key properties of the synthesized catalyst and compares them with the data reported for the original commercial catalyst used by Laudenschleger et al.[17] and to the original report of the reproduced benchmark catalyst synthesis by Schumann et al.[21] The comparison shows that the synthesized catalyst represents very well the expected properties of the commercial CZA. The here-reported reproduction of the benchmark synthesis thus resulted in a similar catalyst with only slightly lower values in the specific surface area of the calcined precatalyst and N_2O-chemisorption capacity of the reduced catalyst. This could be caused by enhanced CuO sintering during calcination.

Catalytic Performance in Methanol Synthesis. Methanol synthesis was conducted over the above-described catalysts at 210 °C and 60 bar in a feed composed of 13.5% CO/3.5% CO_2/73.5% H_2/9.5% N_2. To ensure that the catalyst is stable during conversion on the timescale of the gas pulse experimentations, it was operated for more than 100 h under these conditions right after activation. The investigated catalyst lost about 20% activity after reaching the first maximum methanol formation rate (Figure 1). After this drastic loss, the deactivation of CZA decelerated and stabilized at around 70% of its original activity. Such an initial activity drop is typical for Cu-based methanol synthesis catalysts in the first 50 h time on stream.[40,41] Within this time frame, the catalyst may lose up to 60% of its original activity.[41] The main reason is thermally induced Cu particle sintering which can be enhanced if the ZnO spacer additionally is consumed by the in situ formation of $ZnAl_2O_4$ or Zn-OH species due to water formation in CO_2-containing synthesis gas.[23,39,41] The observed deactivation of the CZA catalyst was stronger in the first 20 h than expected from a similar catalyst and similar aging reported by Fichtl et al.[40] resulting in a higher rate constant (k) and order (m) of the deactivation rate (Figure 1). In contrast to the compared deactivation kinetics (Figure 1, power-law fit according to Fichtl et al.[40]), the CZA catalyst stabilized its productivity faster at a methanol formation rate of about 336 μmol g^{-1} min^{-1}, which is in line with previously reported activity data of about 350 μmol g^{-1} min^{-1} of a similar catalyst under similar reaction conditions.[11] The short-term behavior was described quite well by the deactivation data reported by Sun et al.[39] for a similar catalyst and synthesis gas (60% Cu/28% Zn/11% Al; $CO_2/(CO + CO_2) = 0.8$).

After about 130 h time-on-stream, the catalyst was further aged for one more week at 250 °C with a lower flow rate of 26 mL_N min^{-1} under equilibrium-controlled conditions analogous to Fichtl et al.[40] This treatment resulted in a sufficiently stable performance over the time period of the pulsing experiments.

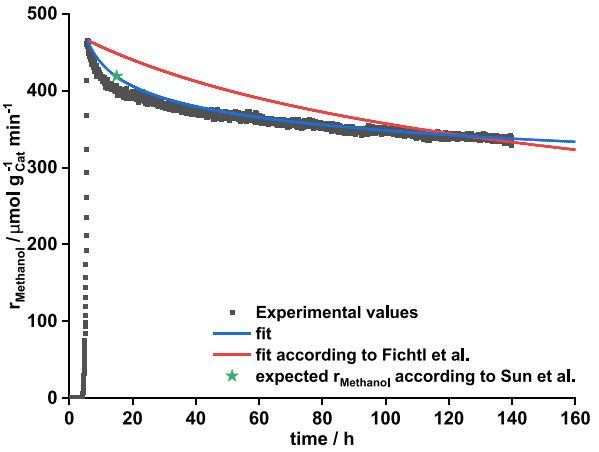

Figure 1. Aging of CZA in a mixed synthesis gas containing CO/CO_2/H_2 under differential reaction conditions. The volume flow was set to 666 mL min^{-1} $g_{Catalyst}^{-1}$ at 60 bar and 210 °C. This procedure was chosen to age the catalyst in the first week while investigating in parallel the initial thermal deactivation under kinetically controlled reaction conditions. The deactivation values were estimated by fitting a power law to the methanol formation rate according to Fichtl et al.[40] The parameters obtained by Fichtl et al.[40] were determined with a similar CZA catalyst at similar reaction conditions (220 °C, 60 bar, 1.39 vol % CO, 3.60 vol % CO_2, 62.68 vol % H_2, and WHSV = 0.51 h^{-1}).[40] The point marked with a star was calculated by the deactivation data reported by Sun et al.[39] for a similar catalyst and synthesis gas (60% Cu/28% Zn/11% Al; $CO_2/(CO + CO_2) = 0.8$). The kinetic parameters are listed in the Supporting Information in Table S3.

High-Pressure Pulse Experiments. After reaching steady-state conversion, the experiments of Laudenschleger et al.[17] were reproduced using the CZA catalyst. In Figure 2, the results of the temporary poisoning by NH_3 are shown using a CO/CO_2/H_2 synthesis gas at 60 bar and 210 °C. The isobaric injection of 1 mL pure N_2 results only in a sharp negative dilution peak in the methanol content of the off-gas (see Figure 2, 0 ppm NH_3). The original methanol amount is recovered immediately. Also, the NH_3-containing pulses cause the methanol content first to decrease to the same lowest level as in the dilution peak due to the same volume which was injected into the upstream gas (Figure 2, e.g., 500 ppm NH_3). However, compared with the dilution effect, reacting probe molecules like NH_3 have an additional effect on the regeneration time, which strongly increases with the increasing amount of pulsed NH_3 (Figure 2, 500 ppm NH_3 vs 2000 ppm NH_3).

This behavior demonstrates a temporary reversible poisoning of the active sites. As it is known[17,42] that ammonia is converted in a stepwise manner under these conditions to monomethylamine (MMA), dimethylamine (DMA), and finally to trimethylamine (TMA), the decelerated formation of methanol can have two contributions: competitive adsorption on the active surface and/or competition of the C_1 intermediates ending up in methylamine and not in methanol. To estimate these contributions, the same experiment can be performed by pulsing TMA instead of NH_3.[17] The decrease in methanol during the injections of different amounts of TMA confirms that this molecule also acts as a reversible poison (Figure 3). As no further methylation is possible in the case of TMA, this effect is clearly caused by the reversible adsorption of TMA on the methanol-forming active

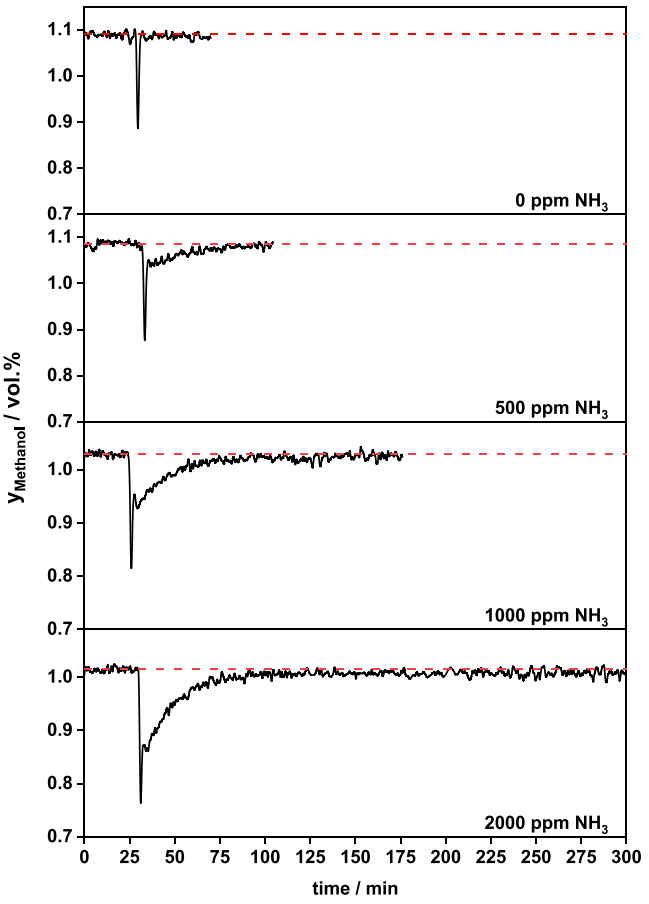

Figure 2. Methanol formation poisoned by injecting 1 mL N_2 containing different amounts of NH_3 into the inlet gas during methanol synthesis in 13.5 vol % CO/3.5 vol % CO_2/73.5 vol % H_2/9.5 vol % N_2 using 200 mg (sieve fraction, 255−300 μm) of the CZA catalyst at 60 bar and 210 °C. To demonstrate the dilution effect, only 1 mL of pure nitrogen was injected into the inlet gas stream (0 ppm NH_3).

sites, as it was also previously described by Laudenschleger et al.[17] This is supported by the TMA profile that was recorded during the pulsing, which inversely resembles the methanol profile when the dilution peak is subtracted. Adsorption, however, is weak enough for TMA to desorb again relatively fast. Thus, the methanol mole fraction is recovered quite fast compared with the same amount of pulsed NH_3. In the case of pulsing 2000 ppm TMA (Figure 3, 2000 ppm TMA), the original methanol formation rate is reached again after about 25 min. For the same amount of NH_3 (Figure 2, 2000 ppm NH_3), the completely recovered methanol content was reached after about 50 min.

We thus conclude in agreement with previous reports that NH_3 has an additional poisoning effect, namely the scavenging of C_1 surface species that are precursors to methanol. It is assumed that NH_3 reacts with an intermediate of methanol synthesis to form TMA.[17] However, this would lead to a stoichiometric consumption of methanol and does not explain the retarded recovery of the original methanol formation rate. The most likely reason is that the adsorption of NH_3 or any intermediate in the reaction pathway to TMA is much stronger than the adsorption of TMA itself.

Interestingly, in the same experiment, but using a CO_2-free syngas feed consisting of CO and H_2, neither a poisoning effect of NH_3 nor a conversion of this probe molecule to TMA was observed, suggesting that rather reactant-like early intermediates in the CO_2 hydrogenation reaction selectively react with NH_3. Regarding the proposed reaction mechanism of CO_2 to methanol,[5,11,43,44] formate species are the possible candidates for this reaction. Therefore, density functional theory (DFT) calculations were conducted to study the hypothesis of the reaction between adsorbed NH_3 and surface formate species and their impact on methanol synthesis.

DFT Calculations. In order to shed light on the influence of NH_3 and the possible reaction intermediates formed during CO_2 hydrogenation, we turned to DFT calculations using two structural models of the active site that have been introduced in an earlier work.[11] As undercoordinated sites have been shown to play an important role in methanol synthesis,[45] stepped Cu surfaces are used to represent the active sites. Zn alloying into the Cu step has also been suggested as a plausible model representing the Cu−ZnO_x synergy.[11] Our two models (see Figure 4) are thus a stepped Cu(211) surface and a fully Zn-decorated Cu(211) step, denoted Cu(211) and ZnCu(211), respectively. We start by investigating the adsorption and activation of NH_3 on these surfaces. Figure 4 shows the free-energy diagram of NH_3 adsorption and activation at 500 K. As shown in Figure 4a, the adsorption of NH_3 is endothermic under these conditions on both surfaces (ΔG^{500K} = 0.24 eV on Cu(211) and 0.30 eV on ZnCu(211)). The activation of NH_3 on these surfaces to produce chemisorbed NH_2* and H* is also slightly endothermic and accompanied by a rather high reaction barrier (1.91 eV for Cu(211) and 1.84 eV for ZnCu(211)). These results indicate that copper as well as Zn-modified Cu surfaces are incapable of activating NH_3 at low temperatures of 500 K, in line with the known fact that Cu is not a good NH_3 decomposition catalyst.[46] During methanol synthesis, the conversion of CO_2 to methanol produces surface oxygen that is subsequently hydrogenated, forming H_2O.[18,47] We investigated the effect of surface oxygen species (O* and OH*) on the activation of NH_3. As can be seen in Figure 4, the presence of O* (see Figure 4b) and to a similar degree OH* (see Figure 4c) lowers the activation barrier of NH_3 dissociation substantially and also makes the reaction step downhill in energy. The reaction barrier for the surface oxygen activated step is 0.71 and 0.91 eV for Cu(211) and ZnCu(211), respectively. We thus speculate that the activation of NH_3 is only possible if oxygen or hydroxyl groups are present on the Cu or Zn−Cu surfaces. This also explains why we do not observe the poisoning effect of NH_3 in dry CO/H_2-containing syngas, as this does not produce any surface oxygen species. The experimentally observed effect of poisoning of TMA is initially similar to that of NH_3 but only in the short term (see experimental observations, Figure 3). Our calculated values for the adsorption free energy of TMA is ΔG^{500K} = 0.21 and 0.3 eV on Cu(211) and ZnCu(211), respectively. The adsorption energies of MMA and DMA are also in the same range. All adsorption energies are summarized in Table 2. As is obvious from the calculated interactions, the adsorption of these molecules proceeds mostly through physisorption. Judging from the adsorption energies of the various ammonia derivatives, there should not be large influences when going from NH_3 to TMA. Experimentally, however, TMA has a less strong poisoning effect than ammonia. In addition, the adsorption free energies are positive, hinting at a very weak poisoning effect, in contrast to the experimental observation.

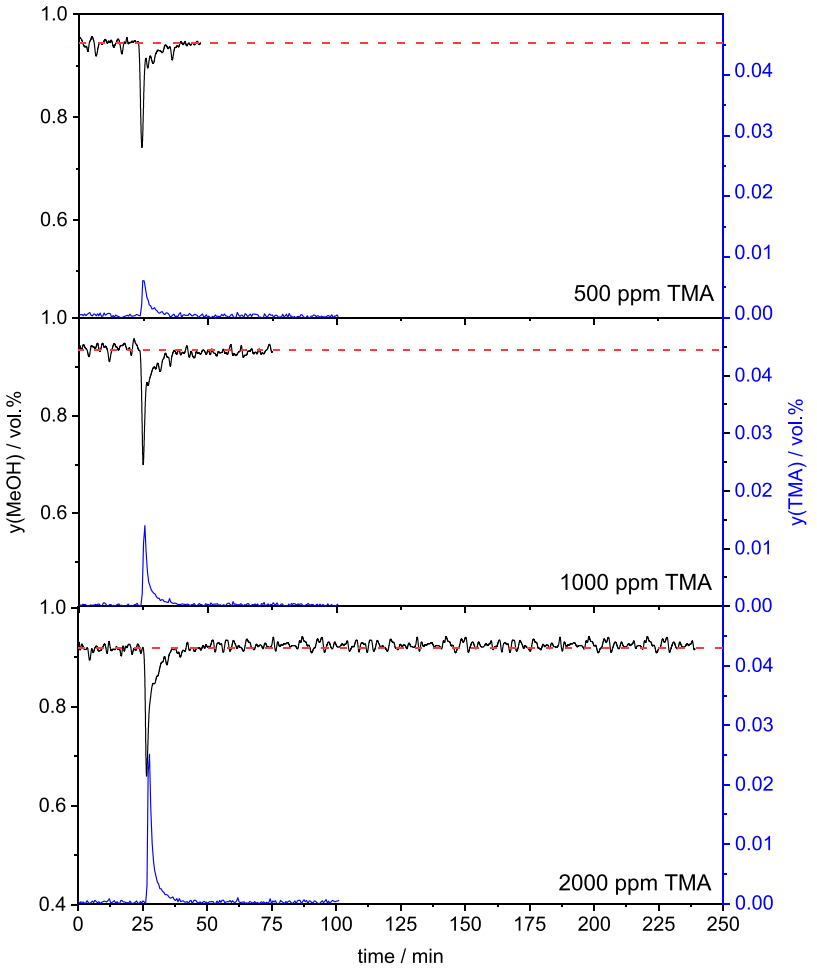

Figure 3. Methanol formation poisoned by injecting 1 mL of N_2 containing different amounts of TMA into the inlet gas during methanol synthesis in 13.5 vol % CO/3.5 vol % CO_2/73.5 vol % H_2/9.5 vol % N_2 using 200 mg (sieve fraction, 255−300 μm) of the CZA catalyst at 60 bar and 210 °C. The methanol content determined by the downstream analytics is illustrated in the upper curve (black, in each graph) and the measured TMA concentration in blue (lower curve in each graph).

We therefore investigated the pathway after ammonia activation with oxygen forming MMA on the surface. Figure 5 depicts the free-energy diagram of the reaction of NH_3 and CO_2, starting with an oxygen-covered surface for both Cu(211) and ZnCu(211). Interestingly, we identified the reactions of CO_2 and NH_2* to NH_2-COO* (carbamate), being both mechanistically feasible (reaction barriers of 0.82 and 1.03 eV for Cu(211) and ZnCu(211), respectively) and downhill in energy. In fact, the chemisorption of carbamate is the lowest energy point in the reaction mechanism, being −0.50 eV (Cu(211)) and −0.46 eV (ZnCu(211)). Further reaction of carbamate through hydrogenation proceeds via NH_2-COOH* and NH_2-CHO* with relatively high barriers. Carbamate is thus formed fast but hydrogenated slowly, eventually resulting in a high coverage of carbamate on the surfaces, which is only reduced slowly once NH_3 is taken out of the feed. This interpretation is supported by the experimentally observed slow recovery of the original methanol activity after NH_3 pulsing in comparison to the fast activity recovery after TMA pulsing (compare Figures 2 and 3). The reported simultaneous hydrogenation of ethylene and CO_2 in the synthesis gas was not limited by activated hydrogen.[17] Contrarily, during NH_3 poisoning, ethylene hydrogenation was unaffected, whereas methanol formation was poisoned but not completely stopped.[17] This observation indicates that hydrogen was activated rapidly and that dissociative hydrogen chemisorption can be excluded as a rate-determining step.

This mechanism is able to explain the strong poisoning effect of ammonia, as carbamate blocks the active site on which formate would be hydrogenated to methanol.

As TMA cannot form a carbamate-like intermediate, the above-described poisoning mechanism cannot be present in agreement with our experimental observation that TMA poisoning is much short-lived, which we ascribe to simple physisorption without the formation of intermediates.

CONCLUSIONS

A combined experimental and theoretical study of the poisoning effect of NH_3 during the conversion of syngas (CO_2/CO/H_2) to methanol over an industrial-type CuZnO:Al catalyst is presented. This catalyst was prepared via co-precipitation and represented in its characteristics an industrial methanol synthesis catalyst. The poisoning effect during methanol synthesis from a CO_2-containing feed gas reported earlier was reproduced, and the interpretation of the experimental results was supported by DFT calculations to identify the stronger poison effect of NH_3 compared with trimethylamine. Extensive DFT calculations on two active site models representative of Cu and Cu/ZnO catalysts were

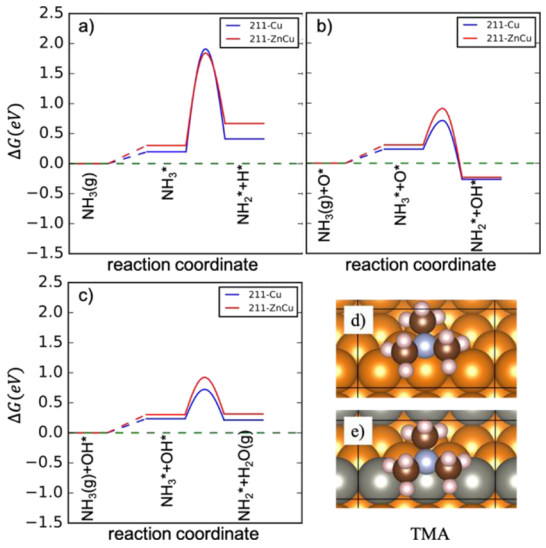

Figure 4. Gibbs free-energy diagrams: (a) NH_3 activation; (b) oxygen-assisted NH_3 activation; and (c) OH-assisted NH_3 activation over Cu(211) and ZnCu(211) at T = 500 K, $p(NH_3)$ = 0.05, $p(H_2)$ = 44 bar, $p(CO_2)$ = 2.1 bar; (d) TMA adsorption geometry on Cu(211) with 0.21 eV binding energy and (e) TMA adsorption geometry on ZnCu(211) with 0.3 eV binding energy.

Table 2. Calculated Adsorption Energies of NH_3, MMA, DMA, and TMA on Cu(211) and ZnCu(211) Surfaces[a]

ΔH adsorption (eV)	NH_3	MMA	DMA	TMA
Cu(211)	−0.63	−0.78	−0.79	−0.75
ZnCu(211)	−0.57	−0.69	−0.74	−0.70

[a]All energies are ZPE-corrected and in eV. Entropic contributions to the free energy are given in the Supporting Information.

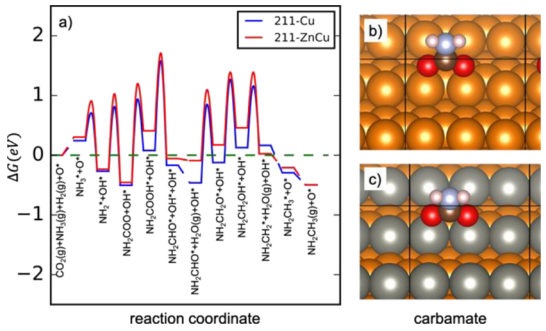

Figure 5. (a) Calculated Gibbs free-energy diagram for NH_3 methylation over Cu(211) and ZnCu(211) in the presence of surface oxygen at T = 500 K, $p(NH_3)$ = 0.05 bar, $p(CO_2)$ = 2.1 bar, and $p(H_2)$ = 44 bar; (b) carbamate at Cu(211) edge; and (c) carbamate at ZnCu(211) edge.

performed, proposing adsorbed carbamate (H_2N-$CO_{2,ads}$) as a possible intermediate blocking the active sites. This investigation shows that carbamate can form readily from the reaction of NH_2* and CO_2 but is a stable species that undergoes further hydrogenation rather slowly, explaining its strong poisoning effect. Importantly, NH_2* can only be formed in the presence of surface oxygen species, such that this effect is not observed for pure CO feeds. TMA as well as NH_3 and the other methylamines do not bind strongly to the surface, according to the calculated adsorption energies. Hence, TMA is not as poisonous as ammonia because it cannot form a strongly bound carbamate species.

AUTHOR INFORMATION

Corresponding Author

Malte Behrens − *Institute of Inorganic Chemistry, University of Duisburg-Essen, Essen 45141, Germany; Institute of Inorganic Chemistry, Christian-Albrecht University of Kiel, Kiel 24118, Germany;* orcid.org/0000-0003-3407-5011; Email: mbehrens@ac.uni-kiel.de

Authors

Benjamin Mockenhaupt − *Institute of Inorganic Chemistry, University of Duisburg-Essen, Essen 45141, Germany; Institute of Inorganic Chemistry, Christian-Albrecht University of Kiel, Kiel 24118, Germany;* Present Address: Department of Chemical Engineering, Catalyst Engineering, Technische Universiteit Delft, Van der Maasweg 9, 2629 HZ Delft, The Netherlands

Philipp Schwiderowski − *Laboratory of Industrial Chemistry, Ruhr-University Bochum, Bochum 44780, Germany*

Jelena Jelic − *Institute of Catalysis Research and Technology, Karlsruhe Institute of Technology, Eggenstein-Leopoldshafen 76344, Germany*

Felix Studt − *Institute of Catalysis Research and Technology, Karlsruhe Institute of Technology, Eggenstein-Leopoldshafen 76344, Germany; Institute for Chemical Technology and Polymer Chemistry, Karlsruhe Institute of Technology, Karlsruhe 76131, Germany;* orcid.org/0000-0001-6841-4232

Martin Muhler − *Laboratory of Industrial Chemistry, Ruhr-University Bochum, Bochum 44780, Germany; Max Planck Institute for Chemical Energy Conversion (MPI CEC), Mülheim an der Ruhr 45470, Germany;* orcid.org/0000-0001-5343-6922

Author Contributions

The manuscript was written through contributions of all authors. B.M.: conceptualization, visualization, data curation, and writing−−original draft preparation; P.S.: conceptualization, visualization, data curation, and writing−−original draft preparation; J.J.: conceptualization, DFT calculations, and writing−−reviewing and editing; F.S.: conceptualization, funding acquisition, supervision, and writing−−reviewing and editing; M.M.: conceptualization, project administration, funding acquisition, validation, and writing−−reviewing and editing; M.B.: conceptualization, project administration, funding acquisition, validation, and writing−−reviewing and editing. B.M. and P.S. contributed equally.

Notes

The authors declare no competing financial interest.

ACKNOWLEDGMENTS

The authors gratefully acknowledge Deutsche Forschungsgemeinschaft (DFG, German Research Foundation) for funding through the priority program SPP 2080 "Catalysts and reactors under dynamic conditions for energy storage and conversion" (project number 406903668), the German Federal Ministry of Education and Research (Bundesministerium für Bildung und Forschung, BMBF, Verbundvorhaben Carbon2Chem, L-2: MeOH Synthese, FKZ: 03EW0006E), the state of Baden-Württemberg for bwHPC (bwUniCluster and JUSTUS, RV bw17D01), and the Mercator Research Centre Ruhr (MERCUR, Pe-2018-0034). Financial support from the Helmholtz Association is gratefully acknowledged. The authors thank Gereon Behrendt for the catalyst synthesis.

ABBREVIATIONS

AAS, atomic absorption spectroscopy; ASE, atomic simulation environment;; BEEF-vdW, Bayesian error estimation functional with van der Waals correlations;; BET, Brunauer–Emmett–Teller surface area of the solid; BJH, Barrett–Joyner–Halenda (pore size determination); Cat, catalyst; C_pdT, enthalpy changes by temperature difference at constant pressure; CZA, copper/zinc oxide/aluminum oxide; DFT, density functional theory; DMA, dimethylamine; E^{tot}, total energy; FFF, given atoms are fixed; FHI-Std., FHI-Standard (CZA catalyst); max, maximum; MeOH, methanol; MMA, mono-methylamine; N_2O-RFC, N_2O reactive frontal chromatography; PAW, projector augmented-wave method; PL, power law (math); rel, relative; S, entropy; TMA, trimethylamine; TPD, temperature-programmed desorption; TPR, temperature-programmed reduction; TTT, given atoms are relaxed; VASP, Vienna ab initio simulation package; XRD, X-ray diffraction; ZPE, zero-point energy

REFERENCES

(1) Menrad, H.; König, A. *Alkoholkraftstoffe*; Springer: Vienna, 2013.
(2) Verhelst, S.; Turner, J. W. G.; Sileghem, L.; Vancoillie, J. Methanol as a fuel for internal combustion engines. *Prog. Energy Combust. Sci.* **2019**, *70*, 43–88.
(3) Räuchle, K.; Plass, L.; Wernicke, H.-J.; Bertau, M. Methanol for Renewable Energy Storage and Utilization. *Energy Technol.* **2016**, *4*, 193–200.
(4) Olah, G. A. Beyond oil and gas: the methanol economy. *Angew. Chem., Int. Ed. Engl.* **2005**, *44*, 2636–2639.
(5) Bowker, M. Methanol Synthesis from CO2 Hydrogenation. *ChemCatChem* **2019**, *11*, 4238–4246.
(6) Bozzano, G.; Manenti, F. Efficient methanol synthesis: Perspectives, technologies and optimization strategies. *Prog. Energy Combust. Sci.* **2016**, *56*, 71–105.
(7) Ren, M.; Zhang, Y.; Wang, X.; Qiu, H. Catalytic Hydrogenation of CO2 to Methanol: A Review. *Catalysts* **2022**, *12*, 403.
(8) Kattel, S.; Ramirez, P. J.; Chen, J. G.; Rodriguez, J. A.; Liu, P. Active sites for CO2 hydrogenation to methanol on Cu/ZnO catalysts. *Science* **2017**, *355*, 1296–1299.
(9) Nakamura, J.; Fujitani, T.; Kuld, S.; Helveg, S.; Chorkendorff, I.; Sehested, J. Comment on "Active sites for CO2 hydrogenation to methanol on Cu/ZnO catalysts". *Science* **2017**, *357*, No. eaan8074.
(10) Kattel, S.; Ramírez, P. J.; Chen, J. G.; Rodriguez, J. A.; Liu, P. Response to Comment on "Active sites for CO2 hydrogenation to methanol on Cu/ZnO catalysts". *Science* **2017**, *357*, No. eaan8210.
(11) Studt, F.; Behrens, M.; Kunkes, E. L.; Thomas, N.; Zander, S.; Tarasov, A.; Schumann, J.; Frei, E.; Varley, J. B.; Abild-Pedersen, F.; et al. The Mechanism of CO and CO2 Hydrogenation to Methanol over Cu-Based Catalysts. *ChemCatChem* **2015**, *7*, 1105–1111.
(12) Kuld, S.; Thorhauge, M.; Falsig, H.; Elkjær, C. F.; Helveg, S.; Chorkendorff, I.; Sehested, J. Quantifying the promotion of Cu catalysts by ZnO for methanol synthesis. *Science* **2016**, *352*, 969–974.
(13) Kuld, S.; Conradsen, C.; Moses, P. G.; Chorkendorff, I.; Sehested, J. Quantification of zinc atoms in a surface alloy on copper in an industrial-type methanol synthesis catalyst. *Angew. Chem., Int. Ed. Engl.* **2014**, *53*, 5941–5945.
(14) Zabilskiy, M.; Sushkevich, V. L.; Palagin, D.; Newton, M. A.; Krumeich, F.; van Bokhoven, J. A. The unique interplay between copper and zinc during catalytic carbon dioxide hydrogenation to methanol. *Nat. Commun.* **2020**, *11*, 2409.
(15) Amann, P.; Klötzer, B.; Degerman, D.; Köpfle, N.; Götsch, T.; Lömker, P.; Rameshan, C.; Ploner, K.; Bikaljevic, D.; Wang, H.-Y.; et al. The state of zinc in methanol synthesis over a Zn/ZnO/Cu(211) model catalyst. *Science* **2022**, *376*, 603–608.
(16) Pandit, L.; Boubnov, A.; Behrendt, G.; Mockenhaupt, B.; Chowdhury, C.; Jelic, J.; Hansen, A.-L.; Saraçi, E.; Ras, E.-J.; Behrens, M.; et al. Unravelling the Zn-Cu Interaction during Activation of a Zn-promoted Cu/MgO Model Methanol Catalyst. *ChemCatChem* **2021**, *13*, 4120–4132.
(17) Laudenschleger, D.; Ruland, H.; Muhler, M. Identifying the nature of the active sites in methanol synthesis over Cu/ZnO/Al2O3 catalysts. *Nat. Commun.* **2020**, *11*, 3898.
(18) Chinchen, G. C.; Waugh, K. C.; Whan, D. A. The activity and state of the copper surface in methanol synthesis catalysts. *Appl. Catal.* **1986**, *25*, 101–107.
(19) Fichtl, M. B.; Schumann, J.; Kasatkin, I.; Jacobsen, N.; Behrens, M.; Schlogl, R.; Muhler, M.; Hinrichsen, O. Counting of oxygen defects versus metal surface sites in methanol synthesis catalysts by different probe molecules. *Angew. Chem., Int. Ed. Engl.* **2014**, *53*, 7043–7047.
(20) Beck, A.; Zabilskiy, M.; Newton, M. A.; Safonova, O.; Willinger, M. G.; van Bokhoven, J. A. Following the structure of copper-zinc-alumina across the pressure gap in carbon dioxide hydrogenation. *Nat. Catal.* **2021**, *4*, 488–497.
(21) Schumann, J.; Lunkenbein, T.; Tarasov, A.; Thomas, N.; Schlogl, R.; Behrens, M. Synthesis and Characterisation of a Highly Active Cu/ZnO:Al Catalyst. *ChemCatChem* **2014**, *6*, 2889–2897.
(22) Deutsches Institut für Normung; *DIN 66136-1:2017-02*; Berlin, **2017**, 1–14.
(23) Fichtl, M.; Hinrichsen, K. O.; Nilges, T.; Köhler, K. *Efficient Methanol Synthesis Catalysts: Long-Term Stability and Deactivation Phenomena*; Universitätsbibliothek der TU München, 2014; pp 1–133.
(24) Kresse, G.; Furthmüller, J. Efficiency of ab-initio total energy calculations for metals and semiconductors using a plane-wave basis set. *Comput. Mater. Sci.* **1996**, *6*, 15–50.
(25) Kresse, G.; Furthmüller, J. Efficient iterative schemes for ab initio total-energy calculations using a plane-wave basis set. *Phys. Rev. B* **1996**, *54*, 11169–11186.
(26) Kresse, G.; Hafner, J. Ab initio molecular dynamics for liquid metals. *Phys. Rev. B* **1993**, *47*, 558–561.
(27) Kresse, G.; Hafner, J. Ab initio molecular-dynamics simulation of the liquid-metal–amorphous-semiconductor transition in germanium. *Phys. Rev. B* **1994**, *49*, 14251–14269.
(28) Bahn, S. R.; Jacobsen, K. W. An object-oriented scripting interface to a legacy electronic structure code. *Comput. Sci. Eng.* **2002**, *4*, 56–66.
(29) Hjorth Larsen, A.; Jørgen Mortensen, J.; Blomqvist, J.; Castelli, I. E.; Christensen, R.; Dułak, M.; Friis, J.; Groves, M. N.; Hammer, B.; Hargus, C.; et al. The atomic simulation environment-a Python library for working with atoms. *J. Phys.: Condens. Matter* **2017**, *29*, 273002.
(30) Wellendorff, J.; Lundgaard, K. T.; Møgelhøj, A.; Petzold, V.; Landis, D. D.; Nørskov, J. K.; Bligaard, T.; Jacobsen, K. W. Density functionals for surface science: Exchange-correlation model development with Bayesian error estimation. *Phys. Rev. B* **2012**, *85*, No. 235149.

(31) Blöchl, P. E. Projector augmented-wave method. *Phys. Rev. B* **1994**, *50*, 17953−17979.
(32) Kresse, G.; Joubert, D. From ultrasoft pseudopotentials to the projector augmented-wave method. *Phys. Rev. B* **1999**, *59*, 1758−1775.
(33) Wellendorff, J.; Silbaugh, T. L.; Garcia-Pintos, D.; Nørskov, J. K.; Bligaard, T.; Studt, F.; Campbell, C. T. A benchmark database for adsorption bond energies to transition metal surfaces and comparison to selected DFT functionals. *Surf. Sci.* **2015**, *640*, 36−44.
(34) Duanmu, K.; Truhlar, D. G. Validation of Density Functionals for Adsorption Energies on Transition Metal Surfaces. *J. Chem. Theory Comput.* **2017**, *13*, 835.
(35) Mallikarjun Sharada, S.; Bligaard, T.; Luntz, A. C.; Kroes, G.-J.; Nørskov, J. K. SBH10: A Benchmark Database of Barrier Heights on Transition Metal Surfaces. *J. Phys. Chem. C* **2017**, *121*, 19807−19815.
(36) Studt, F.; Abild-Pedersen, F.; Varley, J. B.; Nørskov, J. K. CO and CO2 Hydrogenation to Methanol Calculated Using the BEEF-vdW Functional. *Catal. Lett.* **2013**, *143*, 71−73.
(37) Monkhorst, H. J.; Pack, J. D. Special points for Brillouin-zone integrations. *Phys. Rev. B* **1976**, *13*, 5188−5192.
(38) Behrens, M.; Zander, S.; Kurr, P.; Jacobsen, N.; Senker, J.; Koch, G.; Ressler, T.; Fischer, R. W.; Schlogl, R. Performance improvement of nanocatalysts by promoter-induced defects in the support material: methanol synthesis over Cu/ZnO:Al. *J. Am. Chem. Soc.* **2013**, *135*, 6061−6068.
(39) Sun, J. T.; Metcalfe, I. S.; Sahibzada, M. Deactivation of Cu/ZnO/Al2O3 Methanol Synthesis Catalyst by Sintering. *Ind. Eng. Chem. Res.* **1999**, *38*, 3868−3872.
(40) Fichtl, M. B.; Schlereth, D.; Jacobsen, N.; Kasatkin, I.; Schumann, J.; Behrens, M.; Schlogl, R.; Hinrichsen, O. Kinetics of deactivation on Cu/ZnO/Al2O3 methanol synthesis catalysts. *Appl. Catal., A* **2015**, *502*, 262−270.
(41) Kung, H. H. Deactivation of methanol synthesis catalysts - a review. *Catal. Today* **1992**, *11*, 443−453.
(42) Ribeiro, N. F. P.; Henriques, C. A.; Schmal, M. Copper-based Catalysts for Synthesis of Methylamines: The Effect of the Metal and the Role of the Support. *Catal. Lett.* **2005**, *104*, 111−119.
(43) Zhao, Y.-F.; Yang, Y.; Mims, C.; Peden, C. H. F.; Li, J.; Mei, D. Insight into methanol synthesis from CO2 hydrogenation on Cu(111): Complex reaction network and the effects of H2O. *J. Catal.* **2011**, *281*, 199−211.
(44) Porosoff, M. D.; Yan, B.; Chen, J. G. Catalytic reduction of CO_2 by H_2 for synthesis of CO, methanol and hydrocarbons: challenges and opportunities. *Energy Environ. Sci.* **2016**, *9*, 62−73.
(45) Behrens, M.; Studt, F.; Kasatkin, I.; Kuhl, S.; Havecker, M.; Abild-Pedersen, F.; Zander, S.; Girgsdies, F.; Kurr, P.; Kniep, B. L.; et al. The active site of methanol synthesis over Cu/ZnO/Al2O3 industrial catalysts. *Science* **2012**, *336*, 893−897.
(46) Lucentini, I.; Garcia, X.; Vendrell, X.; Llorca, J. Review of the Decomposition of Ammonia to Generate Hydrogen. *Ind. Eng. Chem. Res.* **2021**, *60*, 18560−18611.
(47) Fujitani, T.; Saito, M.; Kanai, Y.; Kakumoto, T.; Watanabe, T.; Nakamura, J.; Uchijima, T. The Role of Metal-Oxides in Promoting a Copper Catalyst for Methanol Synthesis. *Catal. Lett.* **1994**, *25*, 271−276.